Research Article | Vol. 27, No. 4 | 18 Feb 2019 | OPTICS EXPRESS A148
Optics EXPRESS

Near-infrared optics of nanoparticles embedded silica thin films

YANPEI TIAN,[1] ALOK GHANEKAR,[1] LIJUAN QIAN,[2] MATTHEW RICCI,[3] XIAOJIE LIU,[1] GANG XIAO,[2] OTTO GREGORY[3] AND YI ZHENG[1,*]

[1]*Department of Mechanical, Industrial and Systems Engineering, University of Rhode Island, Kingston, RI 02881, USA*
[2]*Department of Physics, Brown University, Providence, RI 02912, USA*
[3]*Department of Chemical Engineering, University of Rhode Island, Kingston, RI 02881, USA*
[*]*zheng@uri.edu*

Abstract: This work investigates experimentally the near-infrared optical properties of SiO_2 thin film embedded with tungsten (W) nanoparticles at varying volume fractions. The samples are prepared by using the technique of magnetron sputtering. The formation and distribution of W nanoparticles are characterized using transmission electron microscopy, and the volume fraction of W nanoparticles is validated by Auger electron spectroscopy. Near- and mid-infrared diffuse reflectance measurements are conducted using Fourier transform infrared spectroscopy. The samples exhibit wavelength selective optical response in the near-infrared region and are suitable for applications involving selective thermal emitters/absorbers. Measured reflectance data is utilized to estimate the effective dielectric function of the nano-composites. Calculated reflectance spectra in different samples are compared to the measured spectra using the experimentally measured dielectric function of these samples in the near-infrared region. Reflectance spectra after thermal annealing at different temperature are compared to show how the thermal treatment affects the optical properties of samples. Optimized structures are proposed for thermal emitters and absorbers with different volume fractions of W nanoparticles.

1. Introduction

The artificial thermal metamaterials which have selective high emissivity at narrowband or broadband wavelength range show promising potentials in the advanced engineering applications, such as thermophotovoltaics (TPVs), infrared thermal sensing [1–8], thermal diodes [9–12], radiation cooling [13–16], thermal rectification [17–19, 43], biosensors, and chemical sensors [20, 21]. Some materials, such as rare earth doped ceramics, possess selective high emissivity, but they do not show sufficient wavelength selectivity that are suitable for the emerging engineering applications [22]. Enhancing the wavelength selectivity is achieved through different methods, such as 2D and 3D photonic crystals [23–25], metamaterials and plasmonics [4, 5]. All of these configurations require expensive micro/nanofabrication methods, thus limiting their engineering applications. Mie-metamaterials are one type of artificial materials which utilize Mie resonances of inclusions to shift or control the shape of emission spectra. Based on sub-wavelength-thick thin films embedded with nanoparticles, Mie-metamaterials enjoy the benefit of easy fabrication and the prospect of applications in wavelength selective thermal emitter/absorber [8, 26, 27]. In an earlier report [27], Theoretical studies on optical and emissive properties of Mie-metamaterials by employing the Clausius-Mossotti equation have been performed. However, the Clausius-Mossotti equation is based on the general assumption that the spacing separating the particles is sufficiently large or the filling ratio of the particles to be small. These conditions limit the utility of the theory to actual materials [28]. Experimental investigation of optical properties of Mie-metamaterials has not been performed. It is critical to investigate optical properties of thin film structures

#347215 https://doi.org/10.1364/OE.27.00A148
Journal © 2019 Received 2 Oct 2018; revised 2 Jan 2019; accepted 22 Jan 2019; published 6 Feb 2019

Optics EXPRESS

embedded with nanoparticles for various engineering applications.

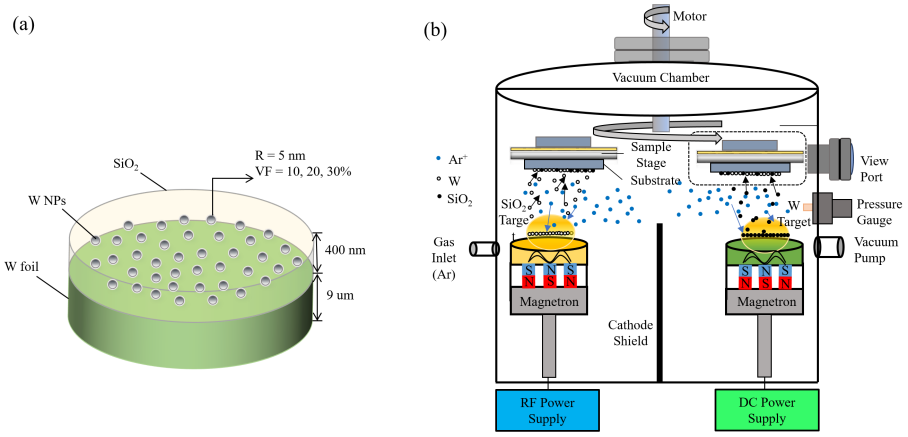

Fig. 1. (a) Schematic of samples consisting of 400 nm-thick SiO_2 film on top of 9 μm W foil as a substrate. SiO_2 thin film is doped with W nanoparticles of 5 nm radius with volume fraction of 10%, 20%, and 30%. (b) Schematic of magnetron sputtering system employed to fabricate samples of W nanoparticles embedded in SiO_2 thin films.

Multi-layered sub-wavelength-thick thin films have been investigated for selective thermal emission properties [29], which can be further enhanced with the inclusion of nanoparticles to control the spectral shift of thermal emission [30–32]. Polymer thin films, e.g., Poly(4-methyl-1-pentene) (PMP) [33] and plydimethylsiloxane (PDMS) [22], show selective thermal emission properties. They can be used in low temperature applications such as radiative cooling, because polymers have relatively low melting point which means their refractive index and temperature are highly dependent [34]. There are several studies pertaining to investigations of the optical properties of polymers. Since ceramics and some metals are chemically stable at high temperatures and have low thermal coefficients of refractive indices, [35], the ceramic thin films embedded with metallic nanoparticles are suitable for high temperature applications, such as Solar Thermoelectric Generators (STEG) and TPVs [8, 36]. SiO_2 and W have high melting points and, recently, they have been used as thermal emitters/absorbers [37–41]. Few experimental investigations are available of the optical properties of SiO_2 thin films embedded with W nanoparticles. As the implantation temperature of TPVs and STEG are around 1,300 K and their emission spectra lie in the near-infrared region, it is important to study the optical properties of W nanoparticles embedded in SiO_2 thin films in the near-infrared region. We prepare a series of 400 nm-thick SiO_2 film embedded with W nanoparticles at various volume fractions (VF) of 10%, 20%, and 30% using the 9 μm-thick W foil as substrates, as illustrated in Fig. 1(a). We measure the reflectance spectra of these samples and refitting these spectra curves according to the Lorentz-Drude model to get the refractive indices of sample in near-infrared region. Based on our results, we propose optimized structures of thermal emitters and absorbers using W nanopartiles with various volume fractions.

2. Samples preparation

We use the technique of magnetron sputtering to prepare our samples with various volume fractions of W nanoparticles embedded in SiO_2 thin films. Two sputtering guns are loaded separately with a W and a SiO_2 target 99.95% purity from Angstrom Science, Inc. The base pressure of the sputtering vacuum chamber is 1×10^{-7} $Torr$, and the Ar sputtering pressure is 4 m$Torr$. We place the substrates on a rotating sample stage (2×2 cm^2 W foils, 9 μm

thickness and 99.95% purity from GoodFellow, Inc.). The stage rotates at a speed of 5.2 rpm. The deposition rate of SiO_2 is 0.247 nm/s at a sputtering power of 150 W, the deposition rate of W is 0.0327 nm/s, 0.076 nm/s, and 0.01063 nm/s at different sputtering power of 5, 13, and 23 W, respectively. Each time as the substrates sweep across the plasma region above a sputtering gun, an ultrathin film of either W or SiO_2 is formed with a thickness much less than a single atomic layer. Since the solubility of W in SiO_2 is negligibly small, the deposited W atoms precipitate into the form of nanoparticles which are naturally embedded in the dielectric medium of SiO_2 thin film. The average size and the volume fraction of the W nanoparticles are determined by the relative fluxes of the W and SiO_2 beam, which are controlled by the individual sputtering power applied to each gun. The sputtering rate for each source is carefully calibrated using the technique of low angle X-ray reflectivity (XRR). The radio frequency (RF) power for the SiO_2 target is fixed at 150 Watt, whereas the direct cuttent (DC) power for the W target is selected at 5, 13, and 23 Watt, corresponding to W volume fractions of 10%, 20%, and 30%, respectively. We use JEM-2100 transmission electron microscopy (TEM) to inspect the W nanoparticles embedded in SiO_2 medium using samples prepared on PELCO silicon nitride TEM grids. The sampe sputtering technology is empolyed to deposited a 30 nm thick W nanoparticles embedded SiO_2 film on the TEM grids.

3. Sample characterization and reflectance measurement

3.1. Film composition characterization

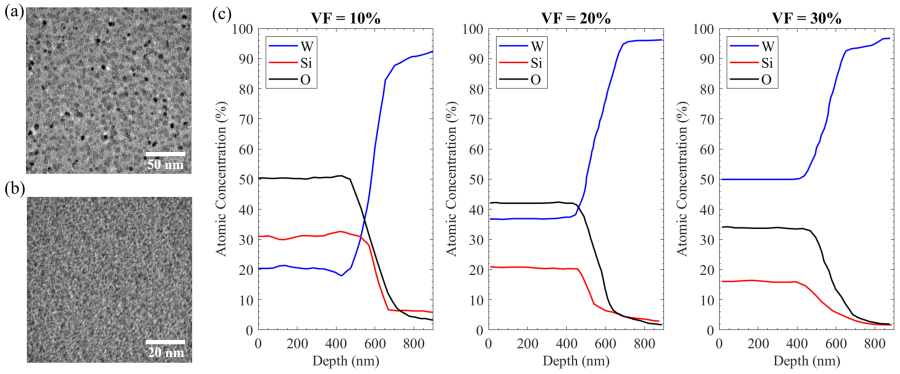

Fig. 2. (a) and (b) TEM images of the fabricated samples with volume fractions 10% and 30%, respectively. (c) Measured atomic concentrations of W, Si, and O at different depth for samples of different volume fractions 10%, 20%, and 30%, using Auger electron spectroscopy.

JEM-2100 Plus Transmission Electron Microscopy is employed to investigate the nanoparticle distribution inside the SiO_2 thin film medium. To analyze the depth dependent atomic concentrations and the volume fractions of W nanoparticles, we use Auger electron spectroscopy (AES) in combination with sputter etching, which is performed inside the Perkin-Elmer Multi-Technique Surface Analysis System 5500. The average atomic concentrations are measured at 5 nm thickness increment. For accurate analysis, samples are cleaned using Ar sputtering to remove surface contaminants, prior to Auger analysis.

3.2. Reflectance measurement

We measure the reflectance spectra using the Jasco 6600 Fourier transform infrared (FTIR) spectrometer with PIKE's diffuse integrated sphere reflectance measurement accessory (Model

number: 660-10740000). Sample is placed on the the top of the accessory facing downwards. The accessory has a spherical shell coated with a highly reflective layer of diffused gold. The light from the interferometer falls on the sample via a gold mirror. Light scattered by the sample is collected by the gold sphere and is eventually captured by the detector. The central mirror can be turned to point at the sphere to take reference measurement of gold (assumed to be 100% reflecting). Angle of incidence on the sample is fixed to 12 °. Nearly 96% of the reflection is specular while about 4% is diffuse. When samples are measured within the near-infrared range, the FTIR spectrometer uses a halogen source as the incident light and the diffuse integrated golden sphere is equipped with an Indium Gallium Arsenide (InGaAs) detector which is highly accurate in the wavelength region of 0.9 μm to 2.6 μm. When samples are measured within the mid-infrared range, a ceramic source is employed and Mercury Cadmium Telluride (MCT) detector with sufficient accuracy in the range 2.5 μm to 15 μm is used together with the diffuse integrated golden sphere. Scan rate was set to 64 with a resolution of 0.4 cm^{-1}. Light scattered from the sample is reflected multiple times before captured by detectors. Each set of reflectance measurement consist of a background scan and five measurements taken at different locations on a sample surface.

3.3. High temperature stability tests

High temperature stability tests are done in a vacuum tube oven with an alumina tube of 5 cm diameter and 80 cm length. The tube is connected to a rotary vane vacuum pump and a vacuum gauge at one end. The rotary van vacuum pump can keep the oven working at 10^{-2} Pa. Samples are put in an alumina crucible boat (100 mm × 30 mm × 20 mm) and positioned in the center of the oven. The thermal annealing temperature of the samples is 400 ℃, 600 ℃, and 800 ℃ for a 24-hour cycle. The reflectance measurement is carried out after the thermal annealing.

4. Results and discussions

4.1. Film composition analysis

Figures 2(a) and (b) shows that W nanoparticles (the dark spots in the figures) are dispersed inside the SiO_2 media. For the sample with a volume fraction of 10%, the average particle size is about 10 nm diameter. Accurate atomic concentrations of silicon (Si), oxygen (O) and W are analyzed as functions of depth using AES together with sputter etching technology. According to Fig. 2 (c), the volume fractions of different samples are calculated to be 9.5% (± 0.5%) , 19.7 % (± 0.3%) and 29.8% (± 0.2%), consistent with the designed volume fraction. Figure 2(c) shows dramatic changes in concentrations around 400 nm, which corresponds to the thickness of the SiO_2 layer as illustrated in Fig. 1(a). Considering the principles of Perkin-Elmer Multi-Technique Surface Analysis System [42], as described in section 3.1, the surface roughness of the 9 μm W foil substrates is large enough that curves of Si, O and W do not rise or fall sharply above 400 nm and they all gradually increase from 400 nm to 600 nm. Relying on the results from the TEM and AES analysis, the distribution and volume fraction of nanoparticles are confirmed as proposed as well.

4.2. High temperature stability results

After performancing the high temperature stability test after a 24-hour cycle, for the sample with a 10% W nanoparticles volume fraction, reflectance measurement shows that the left shift occurs as shown in Fig. 3(a). With the increasing of thermal annealing temperature from 400 ℃ to 800 ℃, the reflectance after thermal annealing has little change within the wavelength range from 0.9 μm to 1.7 μm. Meanwhile, the reflectance drops within the wavelength range from 2 μm to 2.6 μm. For the sample with a 20% W nanoparticles volume fraction, as shown in Fig. 3(b), the reflectance curve shift to the left when the temperature increases from 400 ℃ to 800 ℃ from 0.9

μm to 1.7 μm. The similar reflectance drops are observered from 2 μm to 2.6 μm when thermal annealing temperature increases.

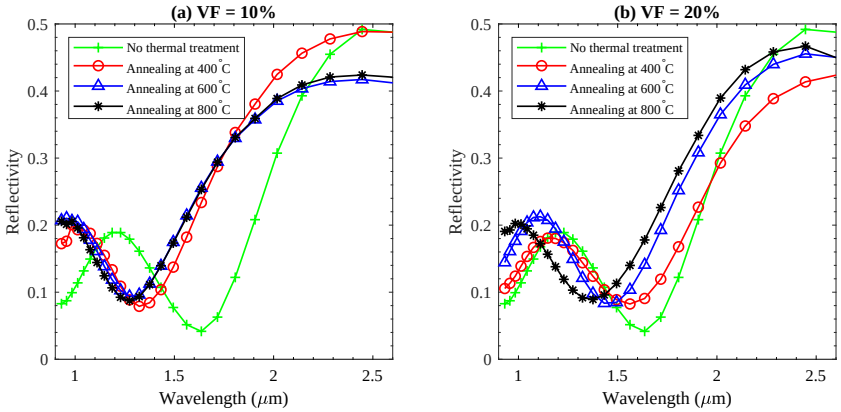

Fig. 3. Comparison of reflectance spectra of samples with different volume fractions 10% and 20%, before and after thermal annealing

4.3. *Estimation of dielectric function*

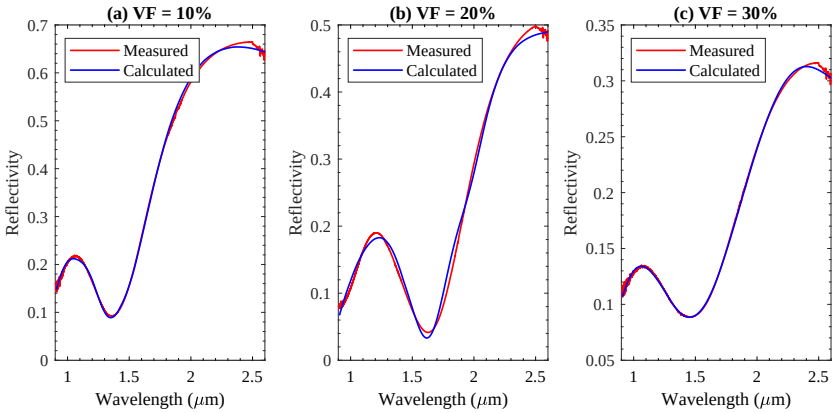

Fig. 4. Comparison of measured and calculated reflectance spectra of samples with different volume fractions 10%, 20%, and 30%, respectively.

A literature has been recently published about how to extract the dielectric function of SU-8 polymer from the reflectance spectra of SU-8 [43]. The same approach is employed to obtain the dielectric function of the nano-composites in this work. The SiO_2 thin films with different volume fractions of W nanoparticles can be considered as three novel materials that are on top of an opaque W layer, and its dielectric function can be extracted from measured reflectance spectra. Dielectric function of these samples are assumed to be in a Lorentz-Drude model given by [44]

$$\varepsilon(\omega) = \varepsilon_\infty + \sum_{k=1}^{N} \frac{s_k}{1 - (\frac{\omega}{\omega_k})^2 - j\Gamma_k(\frac{\omega}{\omega_k})}. \tag{1}$$

Here, s_k, ω_k, Γ_k and j are the strength, resonant frequency, damping factor of kth Lorentz-Drude oscillator and the imaginary unit, respectively. N such oscillators are assumed. ε_∞ is the

Optics EXPRESS

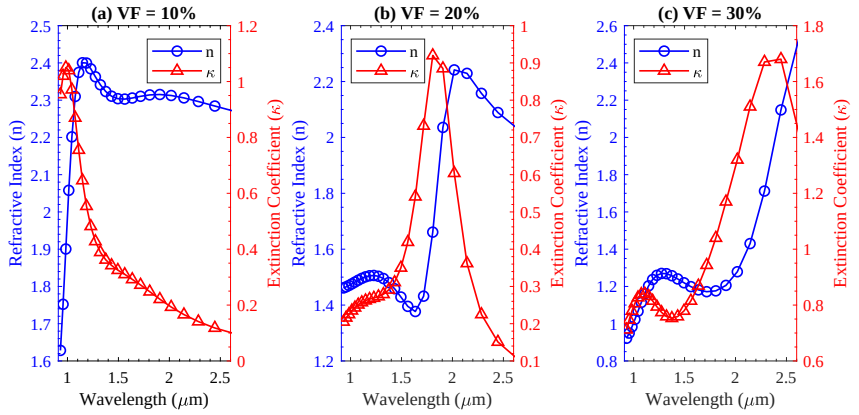

Fig. 5. Estimated refractive indices of fabricated samples with various volume fractions of 10%, 20%, and 30%, respectively.

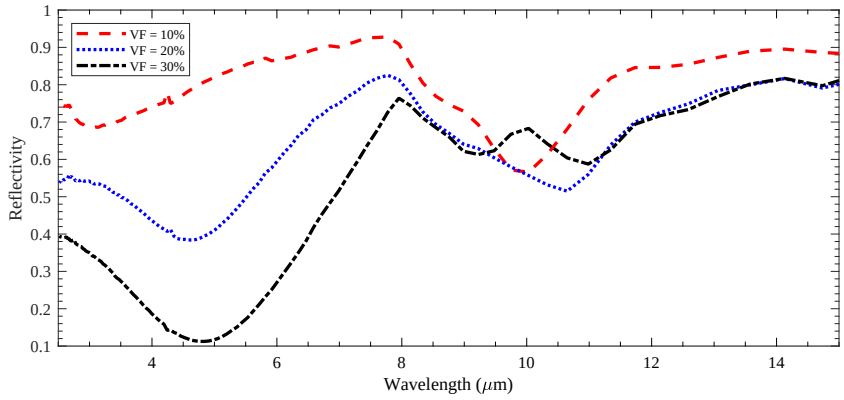

Fig. 6. Reflectance spectra of samples before thermal treatment with different volume fractions 10%, 20%, and 30%, respectively.

contribution from higher frequencies. Since the angle of incidence in the FTIR reflectance measurement is 12°, reflectance values are calculated for that angle of incidence. Dielectric functions of our samples are obtained through fitting several oscillator parameters of the Lorentz-Drude model in order to match the calculated reflectance spectra to the measured spectra. The MATLAB based genetic algorithm is used to obtain an initial guess of oscillator parameters and further optimized by employing MATLAB based constrained optimization function *fmincon*. After obtaining the optimized oscillator parameters, reflectance spectra are calculated and compared with the FTIR measured spectra. The comparison of measured and calculated reflectance spectra are shown in Fig. 4, which validates good matching between measured and calculated reflectance spectra. It validates the fitting oscillator parameters are well defined to show the optical properties in the near-infrared region and can be used in the following proposed thermal emitter/absorber calculations.The oscillator parameters for these samples are provided in Table 1 for different volume fractions of W nanoparticles. Near-infrared optical properties (refractive indices) obtained from refitting of reflectance spectra of these samples are shown in Fig. 5. These optical properties of W nanoparticles embedded silica thin film can be cited in design and calculations about the optical and thermal properties of W nanoparticles embedded

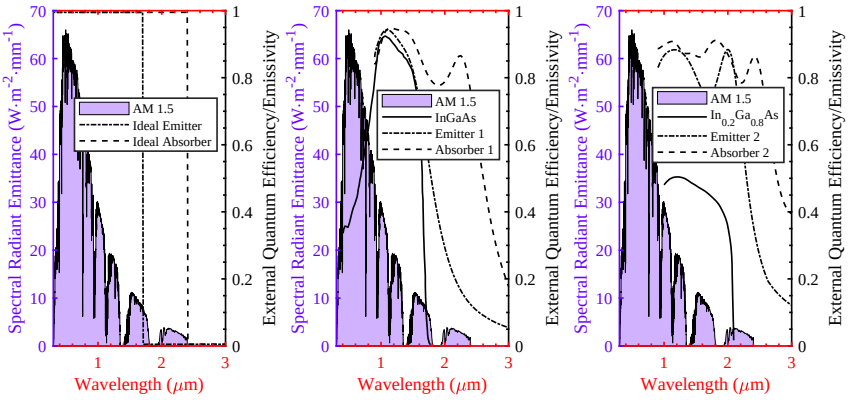

Fig. 7. (a) Incident solar spectrum (AM 1.5, 50 kW^{-2}) and emission spectra of an ideal selective thermal absorber and emitter. (b) and (c) Hemispherical emissivity of the proposed thermal emitter and absorber with different volume fractions 10% and 20%, respectively.

silica thin film in different applications. The method shown in this articles can also be employed to estimate the the optial properties of metal nanoparticles embedded thin film structures.

4.4. *Proposed structure of selective absorber and emitter*

As discussed in section 1 and 4.1, fabricated samples have a high temperature stability and spectrally selective properties in the near-infrared region, which shows the potential to be used in solar thermal applications, such as selective thermal emitter and absorber. Considering Kirchhoff's law which states that for a body in thermal equilibrium, the absorptivity is equal to the emissivity at every wavelength, i.e., $\alpha(\lambda, T) = \epsilon(\lambda, T)$, the inner mechanisms of selective emitter and absorber keep the same. For an ideal emitter in the TPVs, high emissivity below the wavelength corresponding to a certain PV cell's band gap and low emissivity above that wavelength are expected at the same time. For an ideal solar absorber, high absorptivity in visible and near-infrared range (from 0.4 μm to 2.5 μ m) is needed, while keeping a relatively low absorptivity above 2.5 μm. Thus, the emissivity of an ideal selective thermal emitter/absorber should be a step function (as shown in Fig. 7 (a)) with an emissivity of 1 below a certain wavelength and zero emissivity above that wavelength, while having a cut-off between these two [45]. As shown in Fig. 6, the reflectance spectra of samples before thermal annealing shows high reflectivity in the mid-infrared range, especially for the samples with 10% and 20% W inclusions. For the sample with 30% W inclusions, it shows low reflectivity both in the near-infrared and mid-infrared region as shown in 4 (c) and 6, which is not suitable for selective thermal absorber or emitter. According to the near-infrared optical properties of samples in Fig. 5 (a) and (b), four different structures of thermal emitters/absorbers can be proposed here. The sketch of the proposed structure is a layer of SiO_2 thin film on top of a W embedded SiO_2 thin film and the substrate is W film. A top layer of SiO_2 thin film is introduced to act as a surface protection coating, which can enhance the thermal stability at high temperature and anti-reflection coating maximizing emissivity in the visible and near-infrared regions [46]. The optimized thickness of each layer for different emitter/absorber can be found in Table 2. The spectral radiant emittance of the emitters/absorbers are shown in Fig. 5. In Fig. 7(b), the emitter 1 structure is optimized to match an InGaAs solar cell with bandgap of 0.72 eV [27], while in Fig. 7(c), the emitter 2 structure is designed for an $In_{0.2}Ga_{0.8}As$ solar cell with bandgap of 0.52 eV [47]. The hemispherical emissivity of these thermal emitters/absorbers can be evaluated using Equation 1 in the reference [27], as shown in Figs. 7(b) and 7(c).

Optics EXPRESS

Table 1. Lorentz-Drude oscillator parameters of fabricated samples

VF = 10% (ϵ_∞ = 3.5)

k	ω_k	λ_k	s_k	Γ_k
-	(cm^{-1})	(μm)	-	-
1	3,469	1.01	6.032E-01	1.558E-01
2	2,955	1.48	3.760E-01	4.011E-01
3	1,768	2.50	4.175E-05	9.999E-01

VF = 20% (ϵ_∞ = 2.5)

k	ω_k	λ_k	s_k	Γ_k
-	(cm^{-1})	(μm)	-	-
1	3,469	1.03	5.379E-04	1.198E-02
2	2,955	1.88	1.474E-02	2.654E-03

VF = 30% (ϵ_∞ = 1.5)

k	ω_k	λ_k	s_k	Γ_k
-	(cm^{-1})	(μm)	-	-
1	3,459	1.09	2.916E-01	2.554E-01
2	2,963	1.70	9.999E-01	9.998E-01
3	2,963	2.50	9.999E-01	1.625E-01

Table 2. Structure of proposed selective thermal emitter and absorber

	SiO_2	SiO_2 with W NPs	W
	(nm)	(nm)	(nm)
Emitter 1	120	80	1000
Absorber 1	180	700	1000
Emitter 2	60	170	1000
Absorber 2	900	900	1000

5. Conclusion

In summary, the near-infrared optical properties are exploited for W nanoparticles embedded SiO_2 thin film at different volume fractions, which are manufactured by the technique of magnetron sputtering and display optically selective properties. The volume fraction and distribution of W nanoparticles are validated through transmission electron microscopy and Auger electron spectroscopy. High temperature stability tests show samples keep selective reflectivity after thermal treatment, which ensures that W nanoparticles embedded SiO_2 thin film can be utilized in high temperature applications. Lorentz-Drude model parameters are obtained by fitting the measured and calculated reflectance spectra of nanoparticle embedded thin films. Such structures are introduced to enhance the wavelength selective properties in the near-infrared range. The

obtained refractive indices can be cited in design and calculations about the optical and thermal properties of W nanoparticles embedded silica thin film in different applications, such as selective thermal emitter and thermal sensor. This method can also be used to simulate the optical properties of metal nanoparticles embedded thin film structures and serve as predications before fabrications. The proposed selective thermal emitter/absorber structures can be directly applied for solar thermoelectric generators and thermophotovoltaics.

Funding

National Science Foundation (1655221); Institutional Development Award (IDeA) Network for Biomedical Research Excellence from the National Institute of General Medical Sciences of the National Institutes of Health (P20GM103430); National Aeronautics and Space Administration (NNX15AK52A).

Disclosures

The authors declare no conflict of interest.

References

1. A. Lenert, D. M. Bierman, Y. Nam, W. R. Chan, I. Celanović, M. Soljačić, and E. N. Wang, "A nanophotonic solar thermophotovoltaic device," Nat. Nanotechnol. **9**, 126–130 (2014).
2. M. Ghashami, S. K. Cho, and K. Park, "Near-field enhanced thermionic energy conversion for renewable energy recycling," J. Quant. Spectrosc. Radiat. Transf. **198**, 59–67 (2017).
3. H. Wang, V. P. Sivan, A. Mitchell, G. Rosengarten, P. Phelan, and L. Wang, "Highly efficient selective metamaterial absorber for high-temperature solar thermal energy harvesting," Sol. Energy Mater. Sol. Cells **137**, 235–242 (2015).
4. J. Mason, S. Smith, and D. Wasserman, "Strong absorption and selective thermal emission from a midinfrared metamaterial," Appl. Phys. Lett. **98**, 241105 (2011).
5. X. Liu, T. Tyler, T. Starr, A. F. Starr, N. M. Jokerst, and W. J. Padilla, "Taming the blackbody with infrared metamaterials as selective thermal emitters," Phys. Rev. Lett. **107**, 045901 (2011).
6. N. Liu, M. Mesch, T. Weiss, M. Hentschel, and H. Giessen, "Infrared perfect absorber and its application as plasmonic sensor," Nano Lett. **10**, 2342–2348 (2010).
7. S. Ogawa, K. Okada, N. Fukushima, and M. Kimata, "Wavelength selective uncooled infrared sensor by plasmonics," Appl. Phys. Lett. **100**, 021111 (2012).
8. A. Ghanekar, Y. Tian, S. Zhang, Y. Cui, and Y. Zheng, "Mie-metamaterials-based thermal emitter for near-field thermophotovoltaic systems," Materials **10**, 885 (2017).
9. Z. Chen, C. Wong, S. Lubner, S. Yee, J. Miller, W. Jang, C. Hardin, A. Fong, J. E. Garay, and C. Dames, "A photon thermal diode," Nat. Comm. **5**, 5446 (2014).
10. Y. Yang, S. Basu, and L. Wang, "Vacuum thermal switch made of phase transition materials considering thin film and substrate effects," J. Quant. Spectrosc. Radiat. Transf. **158**, 69–77 (2015).
11. Y. Tian, A. Ghanekar, M. Ricci, M. Hyde, O. Gregory, and Y. Zheng, "A review of tunable wavelength selectivity of metamaterials in near-field and far-field radiative thermal transport," Materials **11**, 862 (2018).
12. A. Ghanekar, Y. Tian, M. Ricci, S. Zhang, O. Gregory, and Y. Zheng, "Near-field thermal rectification devices using phase change periodic nanostructure," Opt. Express **26**, A209–A218 (2018).
13. S. V. Boriskina, J. K. Tong, W.-C. Hsu, L. Weinstein, X. Huang, J. Loomis, Y. Xu, and G. Chen, "Hybrid optical-thermal devices and materials for light manipulation and radiative cooling," arXiv preprint arXiv:1509.02516 (2015).
14. H. Iizuka and S. Fan, "Consideration of enhancement of thermal rectification using metamaterial models," J. Quant. Spectrosc. Radiat. Transf. **148**, 156–164 (2014).
15. B. Guha, C. Otey, C. B. Poitras, S. Fan, and M. Lipson, "Near-field radiative cooling of nanostructures," Nano Lett. **12**, 4546–4550 (2012).
16. J.-l. Kou, Z. Jurado, Z. Chen, S. Fan, and A. J. Minnich, "Daytime radiative cooling using near-black infrared emitters," ACS Photonics **4**, 626–630 (2017).
17. Y. Yang, S. Basu, and L. Wang, "Radiation-based near-field thermal rectification with phase transition materials," Appl. Phys. Lett. **103**, 163101 (2013).
18. L. Wang and Z. Zhang, "Thermal rectification enabled by near-field radiative heat transfer between intrinsic silicon and a dissimilar material," Nanoscale Microscale Thermophys. Eng. **17**, 337–348 (2013).
19. A. Ghanekar, Y. Tian, and Y. Zheng, "Photonic metamaterials: Controlling nanoscale radiative thermal transport," in *Heat Transfer-Models, Methods and Applications* (IntechOpen, 2017).
20. C. McDonagh, C. S. Burke, and B. D. MacCraith, "Optical chemical sensors," Chem. Rev. **108**, 400–422 (2008).

Optics EXPRESS

21. M. Pralle, N. Moelders, M. McNeal, I. Puscasu, A. Greenwald, J. Daly, E. Johnson, T. George, D. Choi, I. El-Kady, and R. Biswas, "Photonic crystal enhanced narrow-band infrared emitters," Appl. Phys. Lett. **81**, 4685–4687 (2002).
22. A. Srinivasan, B. Czapla, J. Mayo, and A. Narayanaswamy, "Infrared dielectric function of polydimethylsiloxane and selective emission behavior," Appl. Phys. Lett. **109**, 061905 (2016).
23. S.-Y. Lin, J. Moreno, and J. Fleming, "Three-dimensional photonic-crystal emitter for thermal photovoltaic power generation," Appl. Phys. Lett. **83**, 380–382 (2003).
24. J. Fleming, S. Lin, I. El-Kady, R. Biswas, and K. Ho, "All-metallic three-dimensional photonic crystals with a large infrared bandgap," Nature **417**, 52–55 (2002).
25. E. Hasman, N. Dahan, A. Niv, G. Biener, and V. Kleiner, "Space-variant polarization manipulation of a thermal emission by a sio2 subwavelength grating supporting surface phonon-polariton," in *Conference on Lasers and Electro-Optics* (Optical Society of America, 2005), p. CTuL6.
26. A. Ghanekar, L. Lin, J. Su, H. Sun, and Y. Zheng, "Role of nanoparticles in wavelength selectivity of multilayered structures in the far-field and near-field regimes," Opt. Express **23**, A1129–A1139 (2015).
27. A. Ghanekar, L. Lin, and Y. Zheng, "Novel and efficient mie-metamaterial thermal emitter for thermophotovoltaic systems," Opt. Express **24**, A868–A877 (2016).
28. C.-G. Granqvist and O. Hunderi, "Optical properties of ultrafine gold particles," Phys. Rev. B **16**, 3513 (1977).
29. M. Chirumamilla, A. S. Roberts, F. Ding, D. Wang, P. K. Kristensen, S. I. Bozhevolnyi, and K. Pedersen, "Multilayer tungsten-alumina-based broadband light absorbers for high-temperature applications," Opt. Mater. Express **6**, 2704–2714 (2016).
30. A. R. Gentle and G. B. Smith, "Radiative heat pumping from the earth using surface phonon resonant nanoparticles," Nano Lett. **10**, 373–379 (2010).
31. G. Smith, C. Deller, P. Swift, A. Gentle, P. Garrett, and W. Fisher, "Nanoparticle-doped polymer foils for use in solar control glazing," J. Nanoparticle Res. **4**, 157–165 (2002).
32. A. Heilmann, *Polymer Films with Embedded Metal Nanoparticles*, vol. 52 (Springer Science & Business Media, 2013).
33. Y. Zhai, Y. Ma, S. N. David, D. Zhao, R. Lou, G. Tan, R. Yang, and X. Yin, "Scalable-manufactured randomized glass-polymer hybrid metamaterial for daytime radiative cooling," Science **355**, 1062–1066 (2017).
34. T. Laumer, T. Stichel, T. Bock, P. Amend, and M. Schmidt, "Characterization of temperature-dependent optical material properties of polymer powders," in *AIP Conference Proceedings,* vol. 1664 (AIP Publishing, 2015), p. 160001.
35. P. Timans, "The thermal radiative properties of semiconductors," in *Advances in Rapid Thermal and Integrated Processing* (Springer, 1996), pp. 35–101.
36. D. Kraemer, Q. Jie, K. McEnaney, F. Cao, W. Liu, L. A. Weinstein, J. Loomis, Z. Ren, and G. Chen, "Concentrating solar thermoelectric generators with a peak efficiency of 7.4%," Nat. Energy **1**, 16153 (2016).
37. F. Cao, D. Kraemer, L. Tang, Y. Li, A. P. Litvinchuk, J. Bao, G. Chen, and Z. Ren, "A high-performance spectrally-selective solar absorber based on a yttria-stabilized zirconia cermet with high-temperature stability," Energy Environ. Sci. **8**, 3040–3048 (2015).
38. E. Rephaeli and S. Fan, "Absorber and emitter for solar thermo-photovoltaic systems to achieve efficiency exceeding the shockley-queisser limit," Opt. Express **17**, 15145–15159 (2009).
39. N. Nguyen-Huu, Y.-B. Chen, and Y.-L. Lo, "Development of a polarization-insensitive thermophotovoltaic emitter with a binary grating," Opt. express **20**, 5882–5890 (2012).
40. N. Nguyen-Huu, J. Pištora, and M. Cada, "Wavelength-selective emitters with pyramid nanogratings enhanced by multiple resonance modes," Nanotechnology **27**, 155402 (2016).
41. H. Wang, J.-Y. Chang, Y. Yang, and L. Wang, "Performance analysis of solar thermophotovoltaic conversion enhanced by selective metamaterial absorbers and emitters," Int. J. Heat Mass Transf. **98**, 788–798 (2016).
42. G. M. Burke, D. E. Wurster, M. J. Berg, P. Veng-Pedersen, and D. D. Schottelius, "Surface characterization of activated charcoal by x-ray photoelectron spectroscopy (xps): Correlation with phenobarbital adsorption data," Pharm. Res. **9**, 126–130 (1992).
43. A. Ghanekar, M. Ricci, Y. Tian, O. Gregory, and Y. Zheng, "Dynamic optical response of su-8 upon uv treatment," Opt. Mater. Express **8**, 2017–2025 (2018).
44. H. W. Verleur, "Determination of optical constants from reflectance or transmittance measurements on bulk crystals or thin films," J. Opt. Soc. Am. **58**, 1356–1364 (1968).
45. N. P. Sergeant, O. Pincon, M. Agrawal, and P. Peumans, "Design of wide-angle solar-selective absorbers using aperiodic metal-dielectric stacks," Opt. Express **17**, 22800–22812 (2009).
46. V. Rinnerbauer, A. Lenert, D. M. Bierman, Y. X. Yeng, W. R. Chan, R. D. Geil, J. J. Senkevich, J. D. Joannopoulos, E. N. Wang, M. Soljačić, and I. Celanovic, "Metallic photonic crystal absorber-emitter for efficient spectral control in high-temperature solar thermophotovoltaics," Adv. Energy Mater. **4**, 1400334 (2014).
47. J.-Y. Chang, Y. Yang, and L. Wang, "Tungsten nanowire based hyperbolic metamaterial emitters for near-field thermophotovoltaic applications," Int. J. Heat Mass Transf. **87**, 237–247 (2015).